Effective volumetric lattice Boltzmann scheme

Raoyang Zhang, Hudong Chen, Yue Hong Qian, and Shiyi Chen*
Exa Corp., 450 Bedford Street, Lexington, Massachusetts 02420
(Received 11 July 2000; published 24 April 2001)

An efficient fractional volumetric scheme is proposed for lattice Boltzmann method (LBM). By reducing the effective time step, the scheme possesses much better stability particularly for thermal LBM. The same accuracy and simplicity of the standard LBM are preserved for achieving the Navier-Stokes equation. Since the effective viscosity is reduced by the fraction factor *p*, the scheme becomes very effective for simulating high Reynolds number thermal flows.

DOI: 10.1103/PhysRevE.63.056705 PACS number(s): 02.70.−c, 47.11.+j

I. INTRODUCTION

The lattice Boltzmann method (LBM) was proposed a decade ago as an alternative numerical method to traditional computational fluid dynamics (CFD) for simulating complex fluid flows [1–3]. Unlike conventional methods based on macroscopic continuum equations, the LBM starts from mesoscopic kinetic equations, i.e., the Boltzmann equation, to determine macroscopic fluid dynamics. The kinetic nature brings certain advantages over conventional numerical methods, such as easy handling of complex geometries, parallel computation, consistent modeling of subgrid scale physics, and efficient multiphase simulations [4–7].

In the standard lattice Boltzmann method, the well-known evolution equation of particle distribution function with a BGK collision operator can be written as the following:

$$f_i(\mathbf{x}+\mathbf{e}_i\delta t, t+\delta t) = f_i'(\mathbf{x},t) = f_i(\mathbf{x},t) + \Omega_i(f_i(\mathbf{x},t)) \quad (i=0,1,...,M), \tag{1}$$

$$\Omega_i(f_i(\mathbf{x},t)) = -\frac{f_i(\mathbf{x},t) - f_i^{\mathrm{eq}}(\mathbf{x},t)}{\tau}, \tag{2}$$

where $\mathbf{e_i}$ is the given particle velocity and τ is the single relaxation time. The time-evolving procedure includes two sequential steps: (1) a streaming step during which the particle moves to the neighboring node according to its predescribed velocity, and (2) a collision step during which particles at the same node interact with each other in such a way as to increase the local entropy while conserving certain physical quantities, including mass, momentum, and energy.

It has been shown that LBM is second-order accurate in both space and time [3]. Because of its marginal satisfaction of the Courant-Friedrichs-Lewy (CFL) condition in isothermal cases, the standard LBM often encounters numerical instability for low viscosity (small τ, close to 0.5). This problem becomes even more severe in thermal systems [3,8]. Some modifications have been proposed to extend its order of accuracy, stability, and implementation on general meshes [8–10].

In this paper, extending the volumetric concept [11] and the fractional propagation scheme developed previously [12] we present an efficient fractional volumetric scheme to improve the stability of thermal LBM while keeping the accuracy and simplicity of the original LBM. The paper is organized as follows. Section II is devoted to the formulation of the scheme. In Sec. III numerical simulations will be given to verify theoretical results. Conclusion and discussion will be presented in the last section.

II. FORMULATION OF THE FRACTIONAL VOLUMETRIC SCHEME

The basic purpose of the fractional volumetric scheme is, by reducing the particle effective evolution time step, to increase stability, remove unphysical spurious invariants, and achieve lower viscosity so that it is capable of simulating higher Reynolds number flows. Unlike the standard LBM, which transports all particle density in a streaming step to the neighboring site (except rest particles), our scheme propagates one fraction of the density to the neighboring site while the other fraction remains at the original site [12]. The evolution equation of particle distribution function for our new scheme can be expressed as

$$f_i(\mathbf{x},t+\delta t) = p\left[f_i'(\mathbf{x}-\mathbf{e}_i\delta t,t) + \frac{(1-p)}{2}\delta f_i'(\mathbf{x}-\mathbf{e}_i\delta t,t)\right] + (1-p)\left[f_i'(\mathbf{x},t) - \frac{p}{2}\delta f_i'(\mathbf{x},t)\right], \tag{3}$$

$$\delta f_i'(\mathbf{x},t) = \mathbf{e}_i\delta t\cdot\nabla f_i' = f_i'(\mathbf{x}+\mathbf{e}_i\delta t,t) - f_i'(\mathbf{x},t), \tag{4}$$

where p is a parameter determining the fraction of particle propagation. The f_i' stands for the post-collision quantities. Without the $\delta f_i'$ terms in Eq. (3), the scheme is the same as the one of Qian proposed in 1997. The inclusion of $\delta f_i'$ comes from the use of piecewise linear correction to the original piecewise uniform distribution density in a volumetric representation. From a pointwise point of view, in each propagation, the particle on each lattice site cannot arrive at its neighbor sites. It can only move a distance $0 \leqslant p \leqslant 1$ between lattice sites for each time step. Therefore, particle distributions on lattice sites have to be interpolated. First-order interpolation gives Qian's scheme and second-order interpo-

*Also at Department of Mechanical Engineering, Johns Hopkins University, Baltimore, MD 21218.

lation gives the same formulations as Eq. (3). However, the basic physical picture is clearer from volumetric point of view [11]. For simplicity, a one-dimensional case with uniform lattice is considered:

$$\begin{aligned} f_i(x,t+\delta t) &= \int_{x-c_i\delta t/2}^{x+c_i\delta t/2} \tilde{f}(x,t+\delta t)dx \\ &= \int_{x-c_i\delta t/2-pc_i\delta t}^{x-c_i\delta t/2} \tilde{f}(x,t)dx \\ &\quad + \int_{x-c_i\delta t/2}^{x+c_i\delta t/2-pc_i\delta t} \tilde{f}(x,t)dx. \end{aligned} \tag{5}$$

If we assume that the distribution of $\tilde{f}(x,t)$ within each lattice cell is constant, the above integration equation gives Eq. (3) with the $\delta f_i'$ term neglected. If the distribution of $\tilde{f}(x,t)$ is linear instead of uniform, Eq. (5) gives the same formula as Eq. (3) when a forward finite difference scheme is used to calculate the first-order gradient. We should note here that the $\delta f_i'$ term always satisfies the conservation laws exactly and the scheme achieves second-order accuracy. In fact, such an approach is not limited to uniform mesh, and, unlike its pointwise counterpart [10,13], always preserves exact conservations [11].

The scheme can recover the macroscopic Navier-Stokes equations as the standard LBM without any additional terms. Assume that the long-wavelength and low-frequency limits are of interest and the classical Chapman-Enskog expansion can be applied. The lattice units δx and δt can be regarded as small parameters of the same order ε compared with the macroscopic characteristic scales. It leads to the following relations:

$$\frac{\partial}{\partial t} = \varepsilon \frac{\partial}{\partial t_1} + \varepsilon^2 \frac{\partial}{\partial t_2}, \quad \frac{\partial}{\partial x} = \varepsilon \frac{\partial}{\partial x_1}, \tag{6}$$

and

$$f_i = f_i^{\mathrm{eq}} + \varepsilon f_i^{(1)} + \varepsilon^2 f_i^{(2)} + \cdots, \tag{7}$$

$$\Omega_i = \Omega_i^{\mathrm{eq}} + \varepsilon \Omega_i^{(1)} + \varepsilon^2 \Omega_i^{(2)} + \cdots. \tag{8}$$

Following the standard expansion procedure [3], we obtain the first two order equations:

$$\frac{\partial f_i^{\mathrm{eq}}}{\partial t_1} + p\mathbf{e_i}\cdot\nabla_1 f_i^{\mathrm{eq}} = -\frac{f_i^{(1)}}{\tau}, \tag{9}$$

at ε order and

$$\frac{\partial f_i^{\mathrm{eq}}}{\partial t_2} + \left(1-\frac{1}{2\tau}\right)\left(\frac{\partial f_i^{(1)}}{\partial t_1} + p\mathbf{e_i}\cdot\nabla_1 f_i^{(1)}\right) = -\frac{f_i^{(2)}}{\tau}, \tag{10}$$

at ε^2 order. We should note that the above equations have the same forms, upon rescaling of $\mathbf{e}_i$ to $p\mathbf{e}_i$, as the perturbation equations of the standard LBM [Eqs. (15) and (17) in [3]]. (Indeed when $p=1$, the perturbation equations of our volumetric scheme go exactly back to the standard LBM.) In other words, the fractional volumetric scheme recovers the Navier-Stokes equations exactly at the second-order approximation.

The hydrodynamic quantities of fluid density $\rho(\mathbf{x},t)$ and velocity $u(\mathbf{x},t)$ are defined in the following standard way:

$$\rho(\mathbf{x},t) = \sum_i f_i^{\mathrm{eq}}, \tag{11}$$

$$\rho(\mathbf{x},t)\mathbf{u}(\mathbf{x},t) = \sum_i \mathbf{e}_i f_i^{\mathrm{eq}}. \tag{12}$$

To derive the correct macroscopic hydrodynamic equations, we use the standard equilibrium distribution function f_i^{eq} [3]:

$$f_i^{\mathrm{eq}} = \rho\omega_i\left[1+\frac{\mathbf{e}_i\cdot\mathbf{u}}{c_s^2}+\frac{(\mathbf{e}_i\cdot\mathbf{u})^2}{2c_s^4}-\frac{\mathbf{u}^2}{2c_s^2}\right], \tag{13}$$

where w_i are weighting parameters [3] and c_s is the sound speed.

After some algebraic calculation, we arrive at the governing equations,

$$\frac{\partial\rho}{\partial t} + p\nabla\cdot\rho\mathbf{u} = 0, \tag{14}$$

$$\frac{\partial(\rho\mathbf{u})}{\partial t} + p\nabla\cdot(\Pi^{(0)}+\Pi^{(1)}) = 0, \tag{15}$$

where $\Pi^{(n)}$ is the nth-order momentum flux:

$$\Pi^{(0)} = \sum_i \mathbf{e}_i\mathbf{e}_i f_i^{\mathrm{eq}} = P\mathbf{I} + \rho\mathbf{u}\mathbf{u}, \tag{16}$$

$$\Pi^{(1)} = \left(1-\frac{1}{2\tau}\right)\sum_i \mathbf{e}_i\mathbf{e}_i f_i^{(1)} = p\rho\nu[(\nabla_\alpha(\mathbf{u}_\beta)+\nabla_\beta(\mathbf{u}_\alpha)], \tag{17}$$

where $P=c_s\rho$ is the pressure, and $\nu=c_s^2(\tau-\frac{1}{2})$ is the shear viscosity. Rescaling time by letting $t'=pt$, we obtain the following rescaled equations:

$$\frac{\partial\rho}{\partial t'} + \nabla\cdot\rho\mathbf{u} = 0, \tag{18}$$

$$\rho\left[\frac{\partial\mathbf{u}}{\partial t'} + \mathbf{u}\cdot\nabla\mathbf{u}\right] = -\nabla P + p[\nabla\cdot(\rho\nu\nabla\mathbf{u}) + \nabla\rho\nu\nabla\cdot\mathbf{u}]. \tag{19}$$

Since the fractional parameter p is always smaller than 1 in the present scheme, the kinematic viscosity is reduced linearly by p. For a given single particle relaxation time τ, we can achieve simulations of higher Reynolds number. However, the price to pay is that the time step is increased by a factor of $1/p$; therefore, a compromise of higher Reynolds numbers and efficient computing depends on the problems studied.

The second advantage of the new scheme is the improvement of stability. According to previous studies [8,14] the

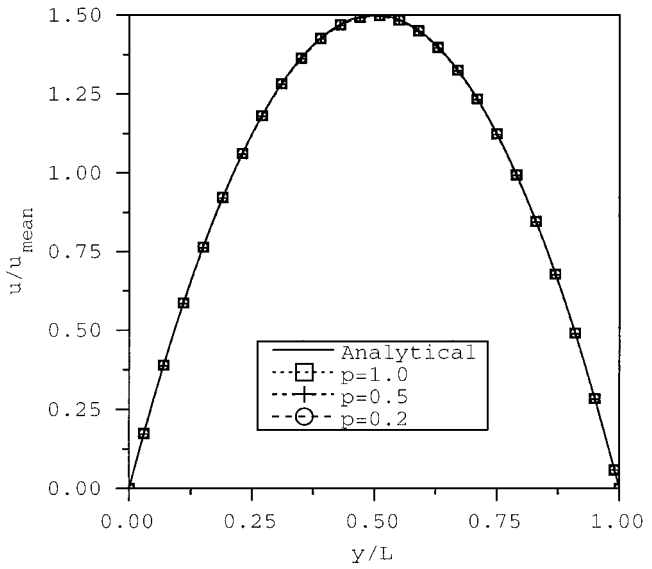

FIG. 1. Steady-state velocity profile in the two-dimensional channel. The solid line is the exact solution. The square is the result of $p=1$. The plus is the result of $p=0.5$. The circle is the result of $p=0.2$. All quantities are dimensionless.

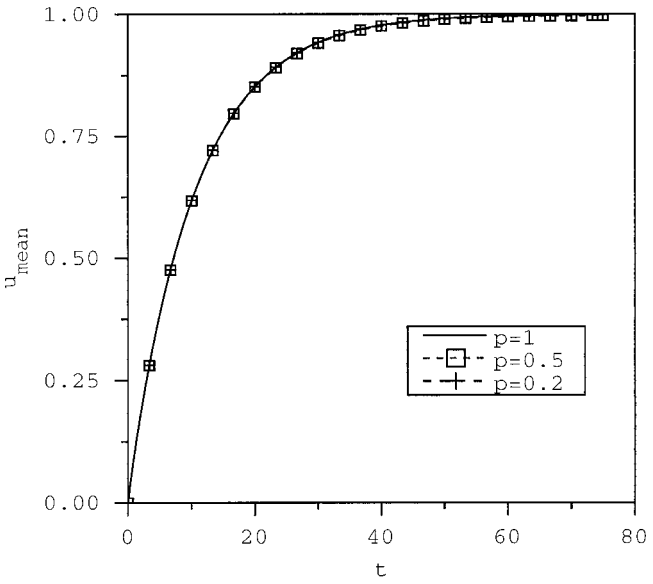

FIG. 2. Time evolution of the mean velocity in the two-dimensional channel. The solid line is the result of $p=1$. The square is the result of $p=0.5$. The plus is the result of $p=0.2$. All quantities are dimensionless.

$\lambda=\Delta t|\mathbf{e}_i|/\Delta x=1$ marginally satisfies the Courant-Friedrichs-Lewy condition for the standard LBM. In the fractional volumetric scheme, the $\lambda=p\Delta t|\mathbf{e}_i|/\Delta x$ is reduced by the factor of p. The CFL condition is better satisfied and for the same Reynolds number isothermal simulation, the scheme is shown to be more stable than the standard LBM.

This advantage is even more important for thermal models because, due to lack of H theorem [15] the stability limitation in the standard LBM is more severe than isothermal models. Special treatment is needed to make the thermal LBM more stable. Previous efforts along this line include the active temperature scalar approaches [3] dynamical rate scheme [9], and so on. In these approaches, either algorithms are complicated or simulations are expensive.

The extension of the fractional volumetric scheme [Eq. (3)] to thermal systems requires at least a three-speed model [9]. The temperature is defined as

$$\rho(\mathbf{x},t)\left(\frac{D}{2}T(\mathbf{x},t)+\frac{1}{2}\mathbf{u}(\mathbf{x},t)^2\right)=\sum_{ij}\ \epsilon_j f_{ij}^{\mathrm{eq}}(\mathbf{x},t). \quad (20)$$

ϵ_j $(=|\mathbf{e}_i|^2/2)$ denotes kinetic energy and the subscript j is the sublattice index representing the different energy levels: Particles with the same speed belong to the same sublattice. The collision operator is the same as Chen, Teixera, and Molvig used in [9] in which a new term is added to the BGK operator to allow for a variable Prandtl number.

$$\Omega_{ij}(\mathbf{x},t)=\sum_{i',j'}M_{ij,i'j'}[f_{i'j'}-f_{i'j'}^{\mathrm{eq}}(\mathbf{x},t)], \quad (21)$$

$$M_{ij,i'j'}=-\frac{1}{\tau}\delta_{ij,i'j'}-\frac{1}{\tau'}\frac{\mathbf{e}_{ij}\cdot\mathbf{e}_{i'j}}{d_j\epsilon_j}\delta_{jj'}. \quad (22)$$

The three-energy-level equilibrium distribution is

$$f_{ij}^{\mathrm{eq}}=\rho g_j(T)\left[1+\frac{\mathbf{e}_{ij}\cdot\mathbf{u}}{T}+\frac{(\mathbf{e}_{ij}\cdot\mathbf{u})^2}{2T^2}-\frac{\mathbf{u}^2}{2T}+\frac{(\mathbf{e}_{ij}\cdot\mathbf{u})^3}{6T^3}-\frac{\mathbf{e}_{ij}\cdot\mathbf{u}}{2T^2}\mathbf{u}^2\right], \quad (23)$$

where i denotes the direction within the sublattice j. $g_j(T)$ is determined by the following constraints from $n=1$ up to $n=3$ [9]:

$$\sum_j\ d_j\epsilon_j^n g_j(T)=\frac{D}{2}\left(\frac{D}{2}+1\right)\cdots\left(\frac{D}{2}+(n-1)\right)T^n, \quad (24)$$

$$\sum_j\ d_j g_j(T)=1, \quad (25)$$

where $D=4$ and $d_j=24$. Similarly to the isothermal case, the effective kinematic viscosity and thermal conductivity are linearly proportional to p,

$$\nu=p(\tau-\tfrac{1}{2})T, \quad (26)$$

$$\kappa=p\left(\frac{2\tau\tau'}{\tau+2\tau'}-\frac{1}{2}\right)3T. \quad (27)$$

III. NUMERICAL VERIFICATION

The first numerical simulation to study the accuracy of the fractional volumetric scheme is the two-dimensional Poiseuille flow, which has the following exact solution:

$$\mathbf{u}=\frac{h^2\mathbf{g}}{2\nu}\frac{y}{h}\left(1-\frac{y}{h}\right), \quad (28)$$

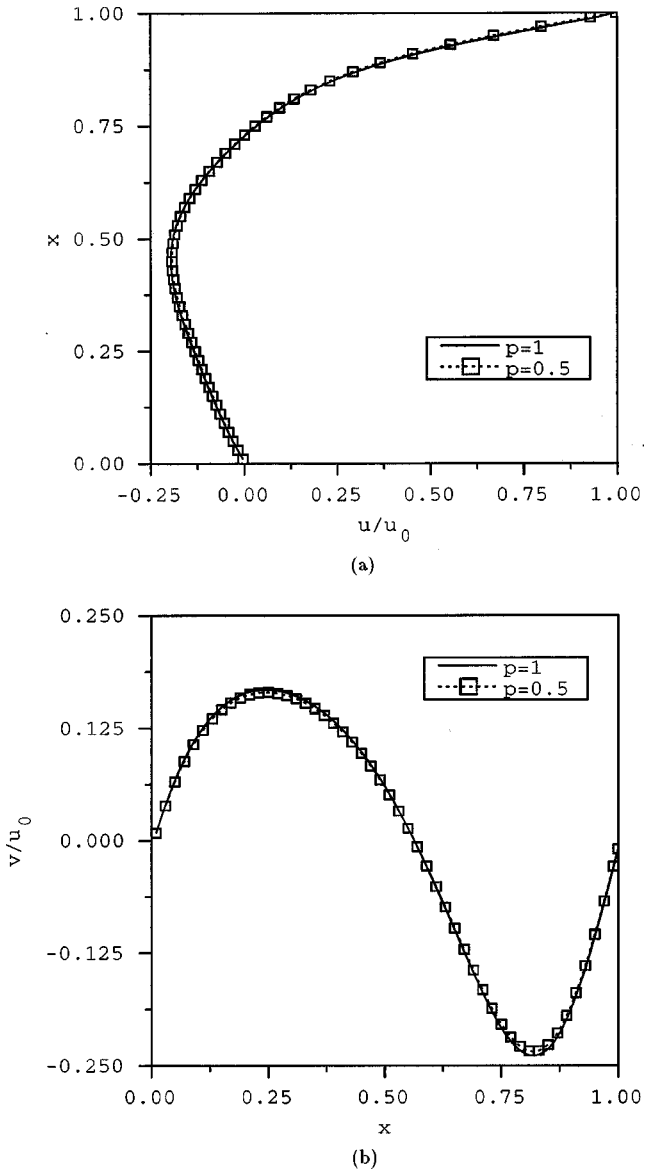

FIG. 3. Velocity profile of u along the vertical centerline of the cavity. (b) Velocity profile of v along the horizontal centerline of the cavity. The solid lines are results of $p=1$. The squares are results of $p=0.5$. All quantities are dimensionless.

where h is the width of the channel and **g** is the gravity. We start from a uniform state of the flow field. With the effect of gravity, the fluid begins to move along the gravitational direction and eventually reaches a steady state when the viscous force balances the gravity. Figure 1 shows the comparison of the steady-state simulation results with the theoretical solution. All simulations have the same viscosity, gravity, and Reynolds number (Re=208) with resolution 60×26. The velocities have been properly normalized by u_{mean} and the distance has been normalized by the channel width. The solid line represents the analytic solution. The squares, pluses, and circles represent simulations with $p=1.0$, 0.5, and 0.2, respectively. To further demonstrate the accuracy of the scheme, we plot the time evolution of the mean velocity in Fig. 2 with solid line, square symbol, and plus symbol,

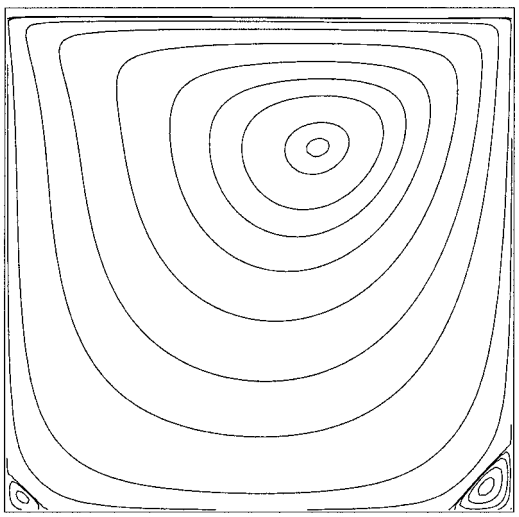

FIG. 4. Stream line of Re=100 and $p=0.5$ in the cavity. Resolution is 100×100.

respectively, for $p=1.0$, 0.5, and 0.2. The time has been normalized by h/u_{mean}. All results are in excellent agreement. The largest error is no more than 0.2%. The above two measures indicate that the fractional scheme gives as good a level of accuracy as the standard LBM.

The second benchmark is numerical simulation of cavity flow. An incompressible fluid is trapped in a square cavity and the flow is driven by a moving lid with a uniform velocity U. This case has been extensively used as a benchmark to study complex physics in a simple geometry and to test numerical schemes. The flow patterns exhibit rich behaviors depending on the Reynolds number, $\mathrm{Re}=UL/\nu$.

There are abundant results in literature using different methods. In particular, Hou *et al.* did a careful investigation in 1995 using the standard LBM [16,17]. Here we compare our results with theirs for Re=100 and 5000, particularly to demonstrate the accuracy and stability of our scheme.

Two values of p, 1 and 0.5, are used. Figure 3 shows the velocity profiles for Re=100 with resolution 100×100. In (a), we plot the velocity profiles for u along the vertical centerline of the box while we plot the velocity profiles for v along the horizontal centerline in (b). The solid lines represent the case of $p=0.5$ and square symbols represent $p=1.0$. The differences between the two cases in both plots are negligible. The velocity profiles compare well with the results of Hou *et al.* [16,17]. In Fig. 4, the contour of the stream function is shown; in addition to the big center vortex, two small secondary vortices appear in the lower corners. The locations of the vortex cores are measured and listed in Table I. All of the locations agree well with the results of Hou *et al.* with 256^2 resolution [16,17]. These agreements indicate again that the fractional volumetric scheme is as accurate as the original LBM at the same resolution for low Re.

We then conduct a similar simulation with the same resolution, 100^2, but much higher Reynolds number, Re=5000. For the standard LBM, i.e., $p=1.0$, the simulation is unstable. However, when we reduce $p=0.5$, the simulation becomes stable and the steady-state solution is plotted in Fig. 5.

TABLE I. Location of vortex centers.

Vortex	Center	Lower left	Lower right	Upper left
Standard (Re=100)	(0.6196,0.7373)	(0.0392,0.0353)	(0.9451,0.0627)	
Volumetric (Re=100)	(0.62,0.73)	(0.04,0.03)	(0.95,0.06)	
Standard (Re=5000)	(0.5176,0.5373)	(0.0784,0.1373)	(0.8078,0.0745)	(0.0667,0.9059)
Volumetric (Re=5000)	(0.52,0.53)	(0.09,0.13)	(0.82,0.08)	(0.06,0.09)

A third secondary vortex appears in the upper left corner. The locations of the center are also listed in Table I.

The results show good agreement with Hou's results with higher resolution. Since the viscosity is effectively reduced by a factor of p in the fractional volumetric scheme, we can achieve higher Reynolds number flows while the standard LBM may become unstable. Furthermore, considering the computational efficiency, the speed of our simulation is increased by a factor of $p(L_{\mathrm{std}}/L_{\mathrm{volm}})^{d+1}$ compared with Hou's simulation speed to get results at the same physical time, which is 8.5 in this case. Here $L_{\mathrm{std}}/L_{\mathrm{volm}}$ stands for the resolution ratio and d is the space dimension.

In the third case, we show the improvement of stability of thermal LBM using our volumetric scheme. What we tested is a two-dimensional pure viscous decaying simulation using the thermal LBM discussed in the preceding section. Superimposed on a constant mean velocity u_0 is a small local random momentum perturbation. Since periodic boundary conditions are used in all directions, the total momentum, total mass, and total energy (kinetic energy+internal energy) are always conserved. In the simulation, the mean flow velocity is $\overline{u_x}=u_0=0.15$, the mean temperature is $\overline{T}=0.5$, the Prandtl number Pr=1, and the amplitude of initial perturbation is 1%. The resolution of the simulation is 50×50.

Figure 6 shows the minimum achievable viscosity ν versus the fraction p. When $p=1$, the corresponding largest Reynolds number achievable is about $\mathrm{Re}=u_0L/\nu=26.8$. When p decreases, the minimum ν decreases nearly exponentially. When $p=0.5$, the largest Reynolds number can be as high as Re=1250. As discussed in the previous section, the Courant number $\lambda=\Delta t|\mathbf{e}_i|/\Delta x=p<1$. The better satisfaction of the CFL condition brings about much better stabilities. In real implementations, the extra cost of memory and gradient calculation in the fractional volumetric propagation for each time step is minor. In fact, the real cost comes from the additional simulation time steps for achieving results at the same physical time when $p<1$. The total simulation time step is scaled by a factor of $1/p$. This tradeoff is very worthy while considering the required stability that we expect for most of the thermal LBM.

Besides the CFL condition, we think another explanation for improved stability may also be plausible. According to the study of Qian in 1997, undesired staggered spurious invariants in LBM could produce large oscillations and lead to instability. The choice of fraction p effectively removes those undesired staggered invariants. Only when $p<1$, can those staggered invariants be damped. Combining computational efficiency and accuracy, the optimal choice of the fraction p is 0.5. Indeed, $p=0.5$ gives significantly lower viscosity and better stability compared to the standard LBM while computational time is doubled.

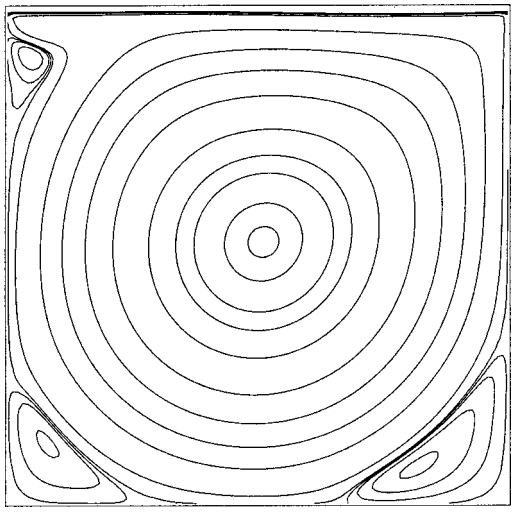

FIG. 5. Stream line of Re=5000 and $p=0.5$ in the cavity. Resolution is 100×100.

IV. CONCLUSION AND DISCUSSION

In this paper, we have proposed a fractional volumetric scheme for LBM. This scheme can fully recover the Navier-

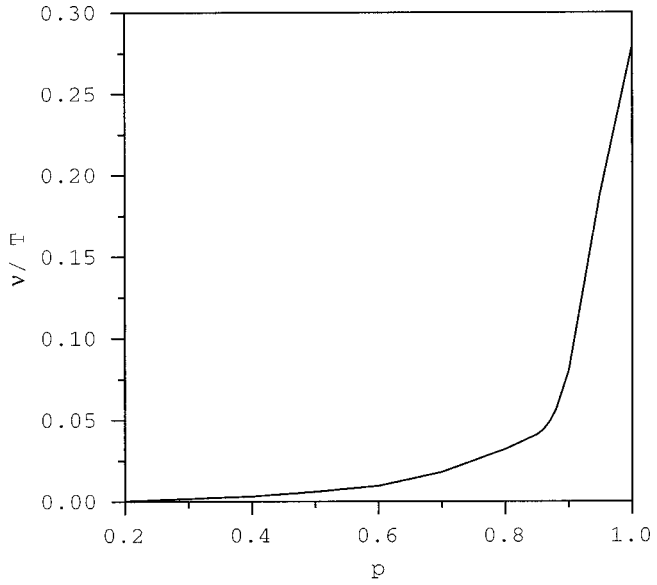

FIG. 6. The achievable minimum viscosity ν vs p in thermal LBM.

Stokes equations and has the same second-order accuracy as the standard LBM. Because the viscosity is effectively reduced by a factor of p, the scheme can simulate higher Reynolds number flows. Also because the typical time step δt is reduced by a factor of p in the fractional volumetric scheme, the CFL condition can be better satisfied. The scheme has a much enhanced stability compared to the standard LBM, especially in thermal situations. This enables us to achieve much higher Reynolds number. The present scheme also effectively removes some unphysical spurious invariants existing in the standard LBM. Compared with a previous fractional model [17], the present scheme need not rescale the velocity field. A straightforward and important application of this scheme is the multiphase thermal models with low viscosity. The fractional volumetric scheme can also be used in formulation of coarse grained models for turbulence [18].

ACKNOWLEDGMENTS

We are grateful to Dr. David Freed, Dr. A. J. Ladd, and Dr. Nick Martys for their useful discussions.

[1] U. Frisch, B. Hasslacher, and Y. Pomeau, Phys. Rev. Lett. **56**, 1505 (1986).
[2] R. Benzi, S. Succi, and M. Vergassola, Phys. Rep. **222**, 145 (1992).
[3] S. Chen and G. D. Doolen, Annu. Rev. Fluid Mech. **30**, 329 (1998).
[4] D. H. Rothman and S. Zaleski, Rev. Mod. Phys. **66**, 1417 (1994).
[5] X. Shan and H. Chen, Phys. Rev. E **47**, 1815 (1993).
[6] M. Swift, W. Osborn, and J. Yeomans, Phys. Rev. Lett. **75**, 830 (1995).
[7] X. He, S. Chen, and R. Zhang, J. Comput. Phys. **152**, 642 (1999).
[8] N. Cao, S. Chen, S. Jin, and D. Martinez, Phys. Rev. E **55**, 2124 (1997).
[9] H. Chen, C. Teixeira, and K. Molvig, Int. J. Mod. Phys. **8**, 675 (1997).
[10] H. He and G. D. Doolen, Phys. Rev. E **56**, 434 (1997).
[11] H. Chen, Phys. Rev. E **58**, 3955 (1998).
[12] Y. H. Qian, Int. J. Mod. Phys. **8**, 753 (1997).
[13] X. He, L. Luo, and M. Dembo, J. Comput. Phys. **129**, 357 (1996).
[14] J. D. Sterling and S. Chen, J. Comput. Phys. **123**, 196 (1996).
[15] H. Chen and C. Teixeira, Comput. Phys. Commun. **129**, 21 (2000).
[16] S. Hou, Ph.D. thesis, Kansas State University, Kansas (1995).
[17] S. Hou, Q. Zou, S. Chen, G. D. Doolen, and A. C. Cogley, J. Comput. Phys. **118**, 329 (1995).
[18] H. Chen, S. Succi, and S. Orszag, Phys. Rev. E **59**, 2527 (1999).